PCCP

Structural Change Dynamics of Heteroleptic Cu(I) complexes Observed by Ultrafast Emission Spectroscopy

Structural Change Dynamics of Heteroleptic Cu(I) complexes Observed by Ultrafast Emission Spectroscopy

Masashi Sanga[1], Kosuke Nakamura[1], Munetaka Iwamura[1]*, Koichi Nozaki[1], Hiroyuki Takeda[2]*,Yu Monma[3] and Osamu Ishitani[3,4]

[1]Department of Chemistry, Graduated School of Science and Engineering, University of Toyama, 3190, Gofuku, Toyama-shi, Toyama 930-8555, Japan

[2]Division of Molecular Science, Faculty of Science and Technology, Gunma University, 1- 5-1 Tenjin, Kiryu-shi, Gunma 376-8515, Japan

[3]Department of Chemistry, School of Science, Tokyo Institute of Technology, 2-12-1-NE-1 O-Okayama Megoro-ku, Tokyo 152-8550, Japan

[4]Department of Chemistry, Graduate School of Advanced Science and Engineering, Hiroshima University, 1-3-1 Kagamiyama, Higashi-Hiroshima, Hiroshima 739 8526, Japan

Abstract

 $[Cu(I)(dmp)(P)_2]^+$ (dmp =2,9-dimethyl-1,10-phenanthroline derivatives; P = phosphine ligand) is one of the most promising photosensitizers used in a photo-catalytic system reducing CO_2, of which quantum yield is as high as 57 %.   In this work, time-resolved emission spectra of the Cu(I) complexes in solutions were investigated using femtosecond fluorescence up-conversion and nanosecond time-resolved emission spectroscopic systems.   The temporal profiles of the emission intensities earlier than 10 ps in the acetonitrile solution were reproduced by tri-exponential function with three-time constants of 0.040 ps, 0.78 ps and 8.0 ps.   We found that only the second time constant is dependent on the solvent (acetonitrile: 0.78 ps, butyronitrile: 1.4 ps), indicating that the 0.78 -ps spectral change is attributed to the structural change of the Cu(I) complex.   The oscillator strengths of transition species are derived from the intensities in the time-resolved emission spectra (species-associated spectra).   Based on the oscillator strengths, we concluded that the 0.040-ps process is the $S_n{\rightarrow}S_1$ internal conversion and the 0.78 -ps process is a structural change in the S_1 state.   The final time constant of 8.0-ps is assigned to that for $S_1{\rightarrow}T_1$ intersystem crossing because the ^3MLCT state (τ_{T1} = 97 ns) is generated after the decay.   A DFT calculation showed that the 0.78 -ps spectral change ($\sim$ 600 cm^{-1} redshift) is attributed to Jahn-Teller distortion around the metal center, and there is a large structural change in ligand, which gives a large Stokes shift in the S_n state (7300 cm^{-1}).

1. Introduction

Photochemistry and photophysics of transition metal complexes have been widely studied in these four or five decades[1-5] because these complexes have suitable properties to use in various photochemical systems such as intense absorption and emission in the visible region assignable to electronic transitions related to charge-transfer excited states.   However, most of these complexes are those of precious metals such as ruthenium, rhenium, and platinum.   Therefore, from a practical point of view, complexes of abundant metals having such photochemical properties are highly required these days.

In this viewpoint, copper (I) complexes with diimine ligands have attracted attention with their photochemical properties that resemble those for well-known tris diimine Ru(II) complexes, i.e. intense metal to ligand charge transfer (MLCT) absorption and long-lived emission in the visible region.[6-9] [10-12]   One of the most characteristic properties of the Cu(I) diimine complexes is a structural change in the excited-states.[13]   A photo-oxidation of the metal center from Cu(I) to Cu(II) due to the MLCT transition induces a structural change to the square planner structure preferred by most Cu(II) complexes from tetrahedral structure preferred by Cu(I) complexes.[14-16]   Since such structural changes are related to the potential energy of the excited-states of the Cu(I) diimine complexes, information about the structural change dynamics is essential for relevant photochemical studies.[12, 17, 18]   Therefore, real-time observations of the excited-state dynamics of the Cu(I) diimine complexes in the femtosecond to picosecond time regions have been performed by number of researchers to elucidate the structural change dynamics.

Studies of the excited-state dynamics of various Cu diimine complexes have been performed by ultrafast spectroscopy such as time-resolved emission[13, 19-21], absorption[22-26], X-ray absorption spectroscopy[18, 27-37], and their combinations[17, 18, 27, 29, 32, 34-39] as well as by theoretical calculations.[37, 40-42]   For $[Cu(dmp)_2]^+$ (dmp = 2,9-dimethyl-1,10-phenanthroline), a typical and standard copper(I) diimine complex, first attempts to observe the ultrafast dynamics was made using femtosecond transient absorption spectroscopy at 2003 by Armaroli and co-workers.[22] Almost at the same time, Lin. X. Chen and co-workers recorded the excited-state structural change by a time-resolved X-rays measurement for $[Cu(dmp)_2]^+$.[32]   In these works, 10-20 ps were proposed as the time constants of structural changes and sub-picoseconds or shorter time constants for those of intersystem crossing for $[Cu(dmp)_2]^+$.   However, different time constants were reported from time-resolved emission spectroscopy.   Nozaki and co-workers claimed ~10 ps as a time constant of the intersystem crossing of $[Cu(dmp)_2]^+$ based on the fluorescence lifetime using picosecond-time resolved emission spectroscopy.[19]   After that, Iwamura et al reported the results of the femtosecond time-resolved fluorescence spectra of $[Cu(dmp)_2]^+$.   They found three time constants of 0.04, 0.7 and 7 ps, and concluded that the structural change process of $[Cu(dmp)_2]^+$ proceeds with a time constant of 0.7 ps because only this component was dependent on the solvent, and the 0.04- and 7-ps components were

assigned to the internal conversion and intersystem crossing, respectively.[13 15, 21, 43]

Ultrafast time-resolved *emission* spectroscopy has various advantages to investigate structural change dynamics of the Cu(I) complexes over other time-resolved spectroscopic techniques. Making assignments of emission bands to transient species is easier than making those of excited-state absorption bands because emission spectroscopy observes electronic transitions from target excited states to the ground state while transient absorption observes those between unknown states.[13, 44] Furthermore, due to the fast intersystem crossing of the transition metal complexes, mixtures of the excited-state singlet and triplet species are sometimes generated in the early time region. In that case, the advantage of fluorescence spectroscopy is conspicuous because fluorescence spectroscopy easily distinguishes signals of the spin-allowed singlet states from that of spin-forbidden triplet states by their intensities, while it is difficult in the cases of the transient absorption and time-resolved X-ray signals. In addition, in the case of $[Cu(dmp)_2]^+$, the difference between the excited-state absorption spectra before and after the structural change was found to be very small.[13, 22, 32] In the case of emission spectra, the spectral change due to structural change was quite clear, which appears as the decay of the emission band at around ~600 nm and rise of that at ~ 700 nm.[23] Therefore, although several time-resolved X-ray measurements have been performed for direct observation of the structural change dynamics of the Cu diimine complexes,[15, 28, 30, 31, 45, 46] information about ultrafast fluorescence spectral changes is still essential to elucidate the excited-state structural changes dynamics of the Cu(I) diimine complexes.[13, 15, 21, 24, 47]

Recently, heteroleptic copper(I) complexes, which have both phosphine and diimine ligands, attract attention because this class of Cu complexes exhibit attractive and advanced photochemical and photophysical properties.[48-58] Especially, $[Cu(I)(dmp)(P)_2]^+$ (dmp = 2,9-dimethyl-1,10-phenanthroline derivatives; P = phosphine ligand) (Fig.1) has a big potential to work as a photosensitizer in photocatalytic systems.[7, 8, 12, 49, 59-61] As reported by Takeda et al, it was found that newly synthesized dimer type Cu(I) complex (Cu-dimer, Figure 1, left) gave the best result of reduction yield of CO_2 (Φ = 57 %) among the $[Cu(I)(dmp)(P)_2]^+$ complexes.[49, 59] Some of the reasons for the high quantum yield may be that the ^3MLCT excited states of $[Cu(I)(dmp)(P)_2]^+$ complexes have longer lifetimes and higher potential energy than ordinal Cu(I) bis diimine complexes.[62] In addition, the smaller structural changes in the excited state may also be important for the photosensitizer. However, the details of excited state dynamics of $[Cu(I)(dmp)(P)_2]^+$ complexes are still unknown.
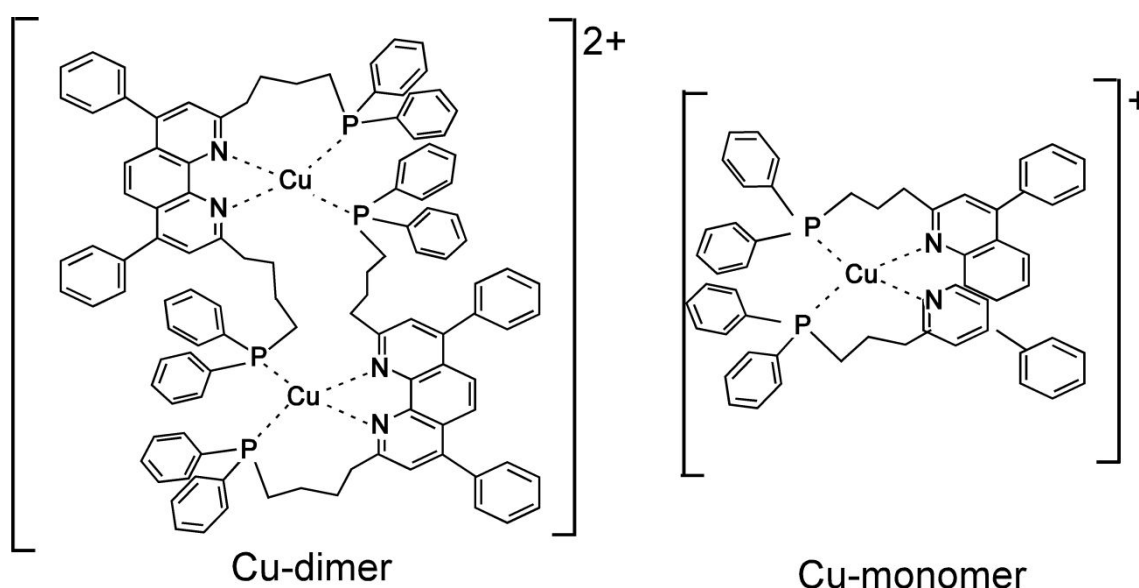
Figure.1   Molecular structure of Cu-dimer&Cu-monomer.

To investigate excited-state dynamics including structural changes of $[Cu(I)(dmp)(P)_2]^+$ complexes, ultrafast time-resolved emission dynamics of Cu-dimer and monomer type of $[Cu(I)(dmp)(P)_2]^+$ (Cu-monomer, Figure 1 right) was observed, where Cu dimer exhibit higher quantum yield for the photo-reduction of CO_2 than for Cu-monomer (ϕ_{CO2} = 6.7 % for Cu-dimer and 2.6 % for Cu-monomer using Fu(II) catalyst).[49]   Femtosecond time-resolved fluorescence spectra were constructed from the spectral data, and we succeeded in making assignments of these excited-state species and time constants such as the internal conversion, the structural change, and the intersystem crossing for Cu-dimer and Cu-monomer.   Theoretical calculations were performed to reveal details of the structural processes.

2.   Experimental Section

2.1. Fluorescence up-conversion measurements

Femtosecond fluorescence measurements were carried out using the lab-made fluorescence up-conversion system reported previously.[21]   Fundamental pulses of a Ti: Sapphire oscillator (Tsunami 810 nm, 1.2W, 80 MHz) were focused on a 0.5 mm thick BBO crystal (θ = 40°). Generated second harmonics (405 nm, ~40 mW) were used as pump pulses for the photo-excitation of samples and residual fundamental pulses were used as gate pulses for the generation of the up-conversion light.   The pump pulses were focused on the sample solution in a 1-mm quartz cell using a concave mirror.   The emission from the sample was focused on a BBO mixing crystal (typically, 0.2 mm, θ = 34° for emission in 500 – 650 nm, 1.0 mm, θ = 44.3° for 675 – 700 nm) via an ellipsoidal mirror (Yamada-Kogaku-Kogyo co.) and a cutoff filter which blocks the excitation light.   The focal length of the ellipsoidal mirror is 39.5 mm from the sample and 212.5 mm from

4

the BBO crystal.   The gate pulses were also focused on the BBO crystal for the up-conversion using another concave mirror.   The path length of the gate pulses was set to mix with the photon from the emission to be recorded using a delay stage with the mirrors.   The angle of polarization of the pump pulses was set by $\lambda/2$ half wavelength plate to detect in magic angle.   The angle of the mixing BBO crystal was set to achieve phase matching between the gated pulses and emission in monitoring wavelength using computer-controlled stepping motors to achieve reproducible measurements.   UV light generated in the mixing crystal was recorded by a photo-multi tube (Hamamatsu Photonics R6353) via a monochromator (Nikon G250), an iris and band-pass filters. The output signal was accumulated in a gated photon counter (Stanford SR400). The full width of half maximum of the Raman scattering signal from the solution was ~160 fs when the 0.2 mm thickness BBO was used as mixing crystal, and ~230 fs in the case of the 1.0 mm crystal.

2.2. Nanosecond time-resolved emission measurements

Emission lifetimes in the nanosecond time region were measured by photoexciting sample solutions with the third harmonic of a Q-switched Nd^{3+}:YAG laser (355 nm, 10Hz, Surelight, Continuum).   The emission was spectrally resolved by a grating monochromator (H20, Jobin Yvon), and detected using a photo-multiplier (R5600u03, Hamamatsu).   The transient signal from the photo-multiplier was accumulated for 160 laser shots on a digitizing oscilloscope (TDS 694C, Tektronix) to obtain the temporal profile of the emission intensity.   The time resolution of this measurement was ~2 ns.

2.3. Steady-state absorption and emission measurements

Absorption spectra were recorded on a commercial spectrometer (MPSInit000, Shimadzu). Steady-state emission spectra were recorded using a labo-build emission spectroscopic system with the excitation at 405 nm.[19]   A 10 mm ×10 mm quartz cell was used for the measurements at R.T. In the case of emission measurements at 77 K, the solvents in the quartz capitally cell were immersed in liquid N_2 in a quartz dewar bottle. The spectral sensitivity in the wavelength region from ~500-800 nm was corrected using a standard lamp and Rhodamine B quantum counter.

2.4. Sample preparation

Cu-dimer was prepared with the same methods represented by the literature.[49] Preparation of Cu-monomer is described in Electronic Supplementary Information (ESI).   All measurements were performed for air-saturated solutions.   The stabilities of the sample during the measurements were checked by comparison with absorption spectra before and after the measurements.

2.5. Theoretical calculations

The optimized geometries and excitation energies of Cu-dimer and Cu-monomer in the lowest triplet (T_1) and ground (S_0) states were calculated with the density functional theory (DFT) and time-dependent DFT (TD-DFT), using a GAUSSIAN 16 program.[63]   DFT calculations were carried

out using a hybrid density functional proposed by Perdew, Burke, and Ernzerhof (UPBE1PBE)[64, 65] and a def2SVP basis set.   The solvent acetonitrile was modeled as a dielectric continuum using a polarisable continuum model (PCM). The solute was set in a cavity surrounded by a solvent-excluded surface. All the parameters used were a default set in GAUSSIAN 16.[63]   Phenyl substituents on the phenanthroline ligands were omitted because the parts were found to be less effective on the calculated parameters.

3.   Results and discussion

3.1. Steady-state spectra

Absorption spectra of Cu-dimer and Cu-monomer in acetonitrile are shown in Figure 2.   Both spectra have broad and intense absorption bands located at around 400 nm. These are assignable to metal-to-ligand charge transfer (MLCT) transitions as described in the previous works.[7, 8, 12, 49] While the MLCT band of Cu-dimer looks to be a single absorption band, Cu-monomer has a characteristic absorption peak at 360 nm with a shoulder at 420 nm.   This indicates that Cu-monomer has two (or more) electronically allowed transitions in this wavelength region.   Thus, it is expected that the MLCT absorption band of Cu-dimer also includes multiple absorption bands. Fitting analysis of the absorption intensity versus wavenumber with multipeak Gaussian line shapes function shows that the MLCT bands of Cu-dimer are not well reproduced by a single absorption band, but well reproduced by the sum of multiple Gaussian bands.   Figure S1 in ESI shows the sum of two Gaussian bands peaked at 381 and 408 nm well reproduce the observed MLCT absorption band in the absorption spectrum of Cu-dimer.

Emission spectra for Cu-dimer and Cu-monomer in acetonitrile solutions at R.T. and 77 K are also shown in Figure 2.   The spectra of Cu-dimer and Cu-monomer have intense broad emission bands which have peaks at around ~600 and ~700 nm, respectively.   The dominant emission bands are assignable to emission from the ^{3}MLCT state.[7]   As in the case of typical Cu(I) complexes with bis-diimine ligands, the emission may include the electronic transition from ^{3}MLCT and thermally activated ^{1}MCLT state, called thermally activated delayed fluorescence (TADF).[6, 66] For simplicity, we call this band as ^{3}MLCT emission.

It is expected that substantial structural changes occur in the excited-state Cu-dimer and Cu-monomer as in the case of typical Cu(I) diimine complexes[15, 32] because there are substantial Stokes shifts (1.0×10^4 cm^{-1} for Cu-dimer and 1.3×10^4 cm^{-1} for Cu-monomer).   The larger Stokes shift of Cu-monomer than that of Cu-dimer indicates that the structural change for Cu-monomer is larger than that for Cu-dimer.   This is also recognized in a comparison of the emission spectra at 77 K to that at R.T.   The emission bands of Cu-monomer at 77 K were observed at a much shorter wavelength (665 nm) than those at R. T (737 nm).   In the case of Cu-dimer, those at 77 K and R. T. are close to each other (618 nm at 77 K and 635 nm at R.T.).   Because Cu-dimer is a dimeric

complex with two metal centers, the structural change in the excited state is expected to occur on only one side and no structural change occurs on the other side.   The Cu complex is linked with the stable another Cu complex, and structural change is expected to be blocked by the stable side in Cu-dimer.
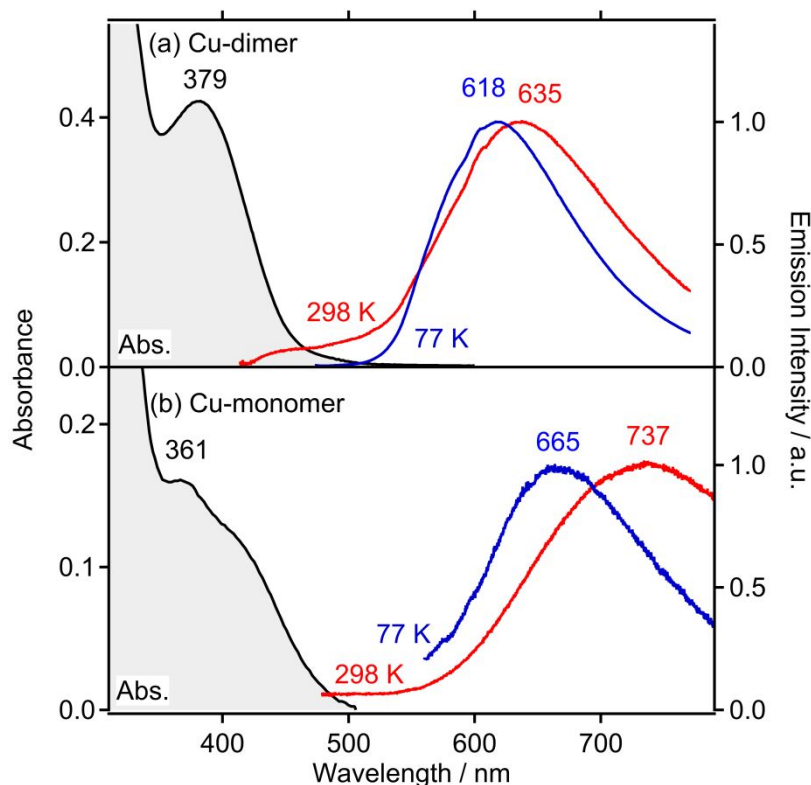

Figure 2.   Absorption and emission spectra for Cu-dimer (a) and Cu-monomer (b) in acetonitrile. Numbers on the spectra indicate peak wavelengths of them.   (λ_{ex} = 405 nm. optical path length = 1 mm, 3.6×10^{-4} mol/dm³ for Cu-dimer and 7.8×10^{-4} mol/dm³ for Cu-monomer)

3.2. Nanosecond time-resolved emission

To observe the excited-state dynamics of the Cu complexes, nanosecond time-resolved emission measurements were performed.   The time-resolved emission spectra for Cu-dimer in acetonitrile are shown in Figure 3.   Immediately after the photo-irradiation at 355 nm, the emission band peaked at 580 nm was observed in the early time region, and the band quickly decays within 20 ns (Figure 3a-1).   The lifetime of this emission is shorter than the time resolution of the measurement system (~2 ns).   After the decay of the short-lived emission, a broad emission band was observed at around ~600 nm (Figure 3a-2).   The emission decays mono-exponentially with a lifetime of 96.6 ns.   The long lifetime (96.6 ns) indicates that the dominant excited species appearing in the later

time region is assignable to the triplet state (^{3}MLCT). Supposing that the fastest components were dominated by emission decay with a time constant of 8 ps (typical lifetime of the Cu complex, which is determined by our femtosecond emission decay. see next section) and the slower one is dominated by that of 97 ns, pre-exponential factors of the fast and the slower components were determined at various wavelengths in 550-700 nm (Figure 3b), where wavelength sensitivity was corrected so that the integrated emission intensity of the time-resolved emission at various wavelengths reproduce the emission spectra of Figure 2. The corrected fast component has an emission peak of 610 nm and the slower one (97-ns component) has a peak of 643 nm. A much higher intensity of the short-lived emission indicates that it is assignable to the fluorescence, and the following long-lived emission is ^{3}MLCT emission.
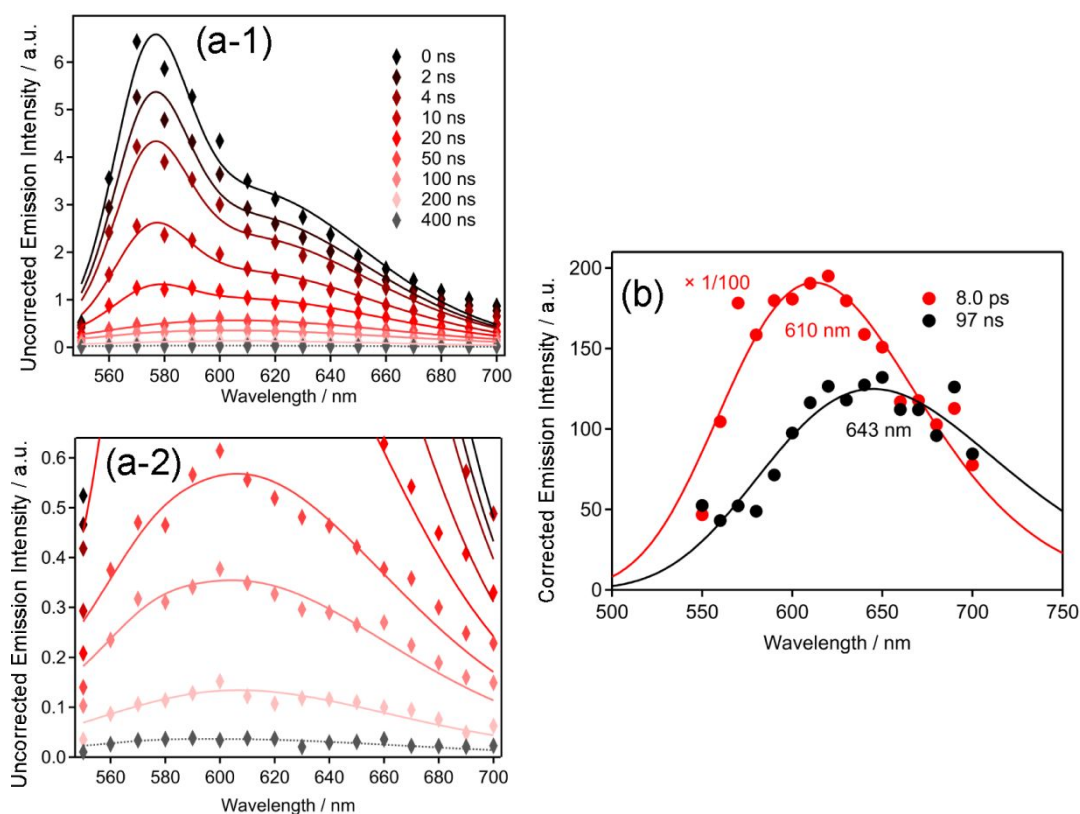
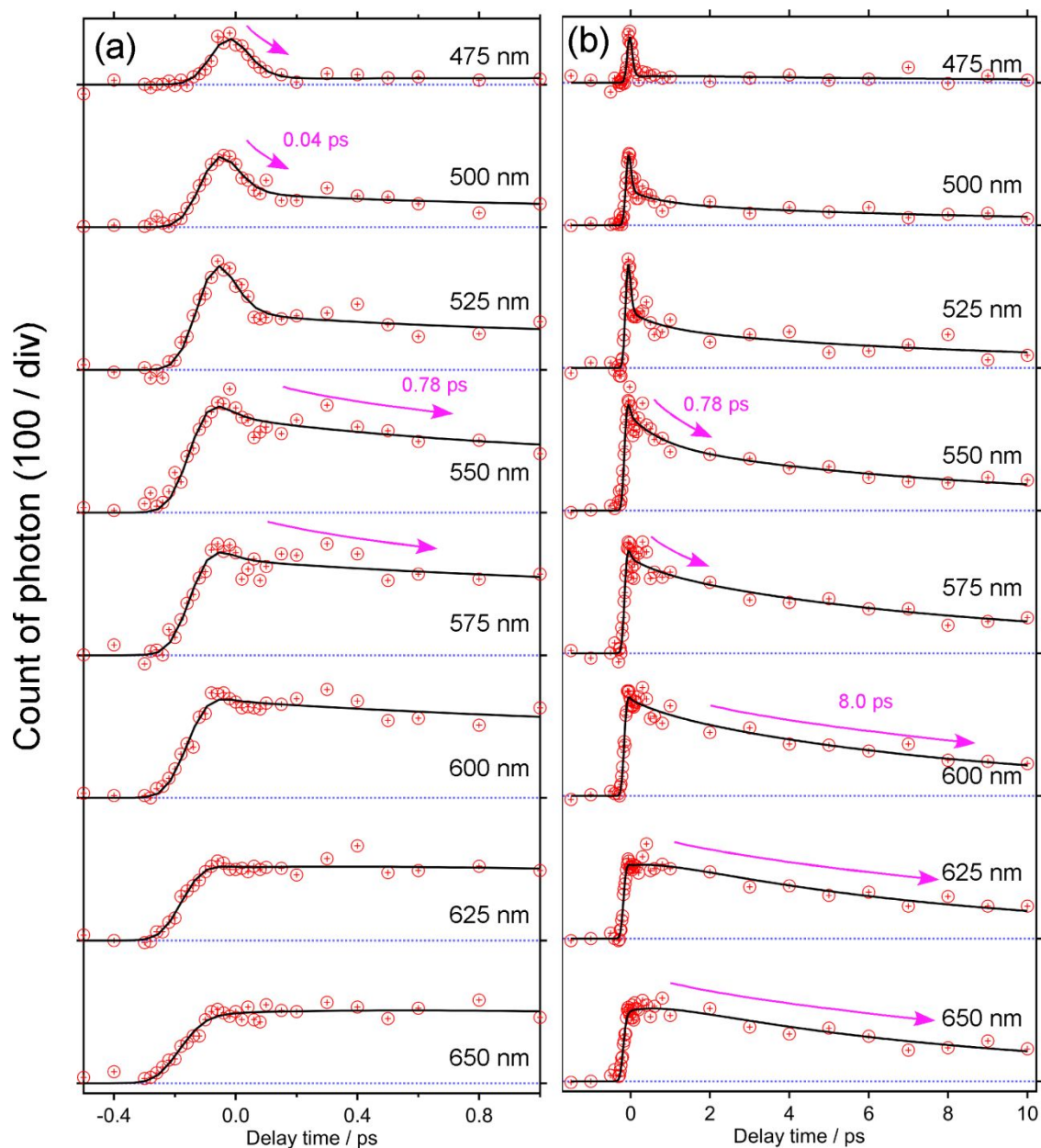**Figure 3.** Nano-second time-resolved corrected emission spectra of Cu-dimer in acetonitrile. (λ_{ex} = 355 nm, 2.1 × 10^{-4} mol/dm^3). Solid lines are fittig curves.
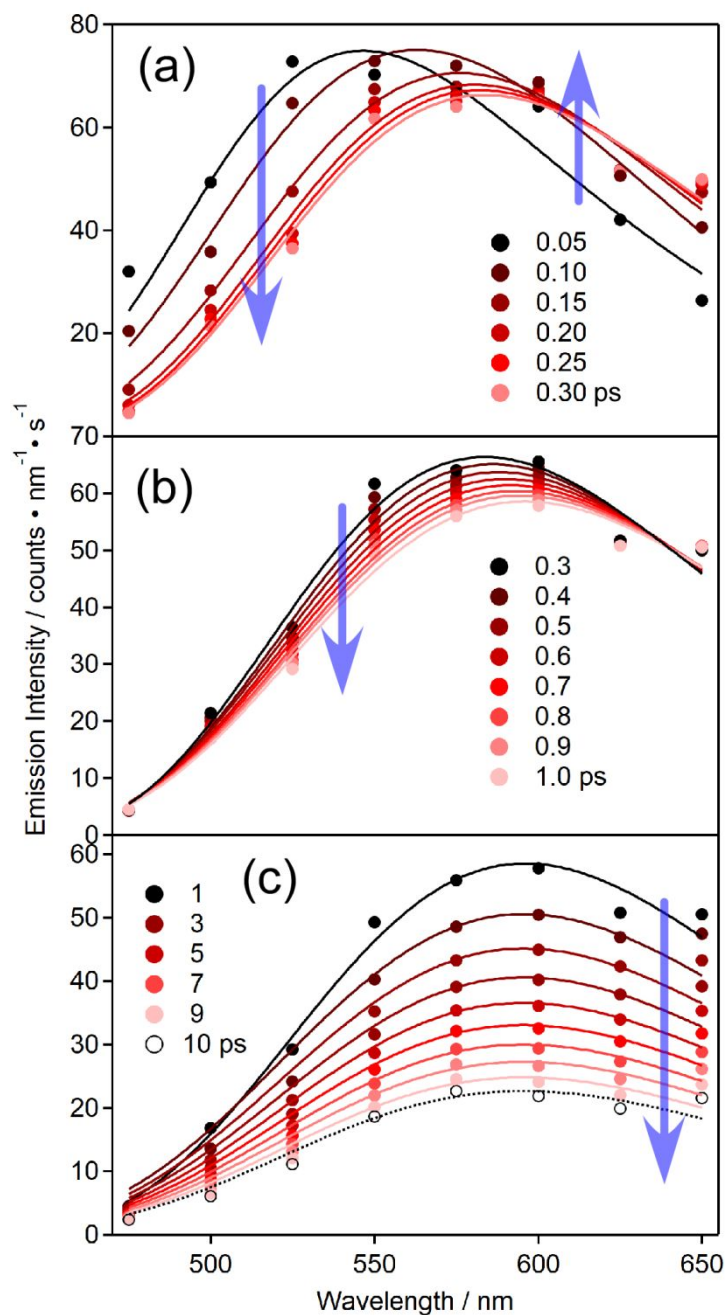
3.3. Femtosecond fluorescence dynamics

The fluorescence spectrum shown in Figure 3b (red line) has a peak around ~600 nm and the peak of the absorption band is located at ~400 nm, i.e. the Stokes shift in Cu-dimer is ~ 200 nm (~ 8.3 × 10^3 cm^{-1}). This suggests that the fluorescence spectrum is dominated by excited-state singlet species

9

after the structural change.   To observe the earlier dynamics in the singlet states including the structural change, femtosecond fluorescence measurements were performed.   Figure 4 shows temporal profiles of the fluorescence intensities for Cu-dimer in acetonitrile up to 10 ps upon photoirradiation with 405-nm light at $t = 0$ ps.   Immediately after the photo-irradiation, short-lived emission was recognized in the wavelength region of 475-525 nm.   It decays quickly within ~0.2 ps.   In the following time region, relatively long-lived emission appears in the wavelength region of 500-650 nm. Decays of the emission with a time constant of ~1 ps were observed in the wavelength region of 550-600 nm.   However, the emission intensity at around 650 nm was almost constant in the 0-1 ps time region.   In the following time region up to ~10 ps, decays of the emission intensity at 500-650 nm with a time constant of ~10 ps were observed.   Global fitting analysis for the temporal profiles at 475-650 nm showed that these profiles were well reproduced by tri-exponential function with three common time constants of 0.040 ± 0.012 ps, (decay at 475-550 nm and rise at 600-650 nm) 0.78 ± 0.29 ps (decay at 500-600 nm), and 8.0 ± 0.6 ps (decay at 500-650 nm).

Figure 4. Temporal profiles of emission intensity (red marker) in the time region within 1 ps (a) and 10 ps (b) for Cu-dimer in acetonitrile. (λ_{ex} = 405 nm, 4.9 × 10^{-4} mol/dm^3) Fitting curves (solid lines) were represented by tri-exponential function using three time constants of 0.040 ± 0.012 ps, 0.78 ± 0.29 ps and 8.0 ± 0.6 ps

Figure 5. Femtosecond time-resolved corrected emission spectra of Cu-dimer in acetonitrile in the time regions of (a) 0.05 - 0.30 ps (b) 0.3 - 1.0 ps (c) 1 - 10 ps. (λ_{ex} = 405 nm, 4.9 × 10^{-4} mol/dm^3) . Solid lines are fittig curves.

Time-resolved fluorescence spectra of Cu-dimer in Figure 5 were built from the temporal profiles of femtosecond time-resolved fluorescence data observed at various wavelengths shown in Figure 4. The correction of the wavelength dependence of the sensitivity of the fluorescence up-conversion system was carried out using a reference sample (Coumarin153)[19] of which fluorescence data was

11

recorded with the same setup using computer controlled phase matching system for the up-conversion crystal.

Initially, the emission band with a peak at around ~520 nm appears in the femtosecond time-resolved emission spectra.   The band decays in the time region of 0-0.3 ps with a time constant of 0.040 ps (Figure 5a).   During this decay, a simultaneous rise of another emission band located around 600-650 nm appears, forming an emission band peaked at around ~580 nm at 0.3 ps. In the following 0.3-1 ps time region, the emission at around 500-600 nm decayed with a time constant of 0.78 ps (Figure 5b).   In the wavelength region longer than 625 nm, emission intensity remains almost constant in this time region.   Therefore, due to the 0.78-ps process, a slight spectral change from ~580 nm to ~600 nm with the iso-emissive point around ~670 nm was recognized in this time region.   In the following time region from 1 to 10 ps, the emission band centered at 600 nm decayed with a time constant of 8.0 ps.

Solvent-viscosity dependence of the time constants is a good marker to determine whether the processes are dominated by structural change or not.[13]   Therefore, femtosecond time-resolved emission for butyronitrile was measured to examine the solvent dependence of emission temporal profiles in acetonitrile (See ESI. Figure S2).   The temporal profiles were also reproduced by three time constants of 0.040, 1.4 and 7.2 ps.   Only the second time constant is changed by solvent (butyronitrile: 1.4 ps; acetonitrile:0.78 ps).   Because the viscosity of butyronitrile is higher than that of acetonitrile (butyronitrile: 0.36 mPas; acetonitrile: 0.59 mPas), it is concluded that the second process is dominated by the structural change process.[13, 20, 21]   The latest 8.0-ps process, of which time constant is independent on the solvent viscosity, is assignable to the intersystem crossing because the ^{3}MLCT emission was observed after the 8.0-ps decay as shown in Figure 3.

Because the excitation light induces the electronic transition to the upper excited state (the initially excited state, S_{Init}), the relaxation process should include an internal conversion process.   However, the time constants of the structural change and the intersystem crossing (0.78 and 8.0 ps in acetonitrile, respectively) were slower than that of typical internal conversions of metal complexes (faster than 0.1 ps).[13, 20, 21]   This indicates that internal conversion from upper singlet states is expected to be finished in the time region later than ~0.3 ps.   Then, the recorded singlet species in the time region of 0.3-10 ps is the lowest singlet excited state, S_1.   The 0.040-ps spectral change is highly likely assignable to internal conversion from the S_{Init} to the S_1 state.   One of the reasons for this is that the time constant is close to that of the typical internal conversion of the Cu(I) complexes.[13]   This will be confirmed by considerably different radiative rate constants before and after the 0.040-ps process as shown in the next section.
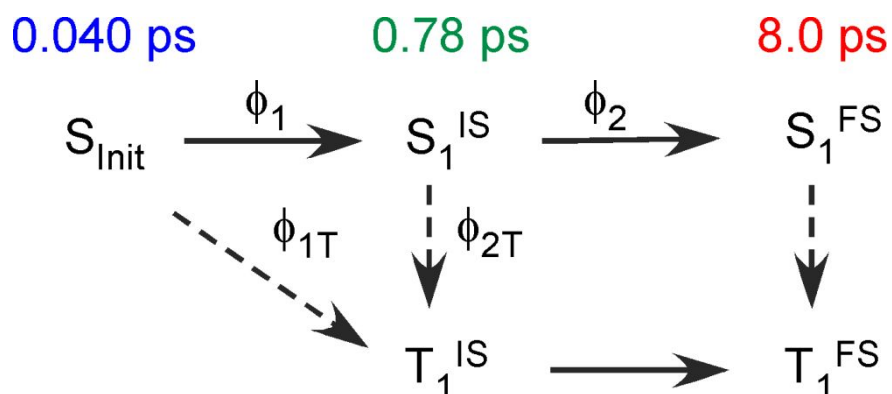
Scheme 1. Proposed relaxation pathways from S_{Init} state of the Cu complexes. S_{init} : Initially excited singlet state. S_1^{IS} : Lowest singlet state (S_1) before the structural change (initial structure) S_1^{FS}: S_1 after the structural change (final structure) T_1^{IS}: Lowest triplet state (T_1) at the initial structure T_1^{FS}: Lowest triplet state (T_1) at the final structure. Quantum yields of the processes are noted near the allows (ϕ_1: $S_{Init} \rightarrow S_1^{IS}$; ϕ_2: $S_1^{IS} \rightarrow S_1^{FS}$; ϕ_{1T}: $S_{Init} \rightarrow T_1^{IS}$; ϕ_{2T}: $S_1^{IS} \rightarrow T_1^{IS}$). Lifetimes of the S_1^{IS}, S_1^{IS} and S_1^{FS} are denoted above the states.

Based on the above assignments, relaxation pathways from photo-excited S_{init} (initially excited singlet state) are represented in Scheme 1. The S_1 states before and after the structural change are S_1^{IS} and S_1^{FS}, respectively. We added paths of intersystem crossing from singlet states to triplet states in this scheme because the processes of the $S_{init} \rightarrow S_1$ and the $S_1^{IS} \rightarrow S_1^{FS}$ may compete with intersystem crossing processes to the triplet states. Then, the yields of these two processes are denoted as ϕ_1 and ϕ_2, respectively. It is worth noting that the lifetime of S_1^{IS} depends on the viscosity of the solvent indicating that it is dominated by the structural change process as mentioned above. This fact indicates that ϕ_2 is close to unity. Based on the model shown in the scheme, we constructed species-associated spectra (SAS) from parameters obtained from the global fitting analysis with the tri-exponential function for the time-resolved fluorescence data in Figure 5. Procedures for the construction of the SAS are essentially the same as that of our previous paper.[13] The SASs of the 0.040-ps emission (blue bands at 520 nm in Figure 6), 0.78 -ps emission (green bands at 580 nm) and 8.0 ps (red band at 620 nm) are fluorescence bands of the $S_{init} \rightarrow S_0$, the $S_1^{IS} \rightarrow S_0$ and $S_1^{FS} \rightarrow S_0$ transitions, respectively.

13
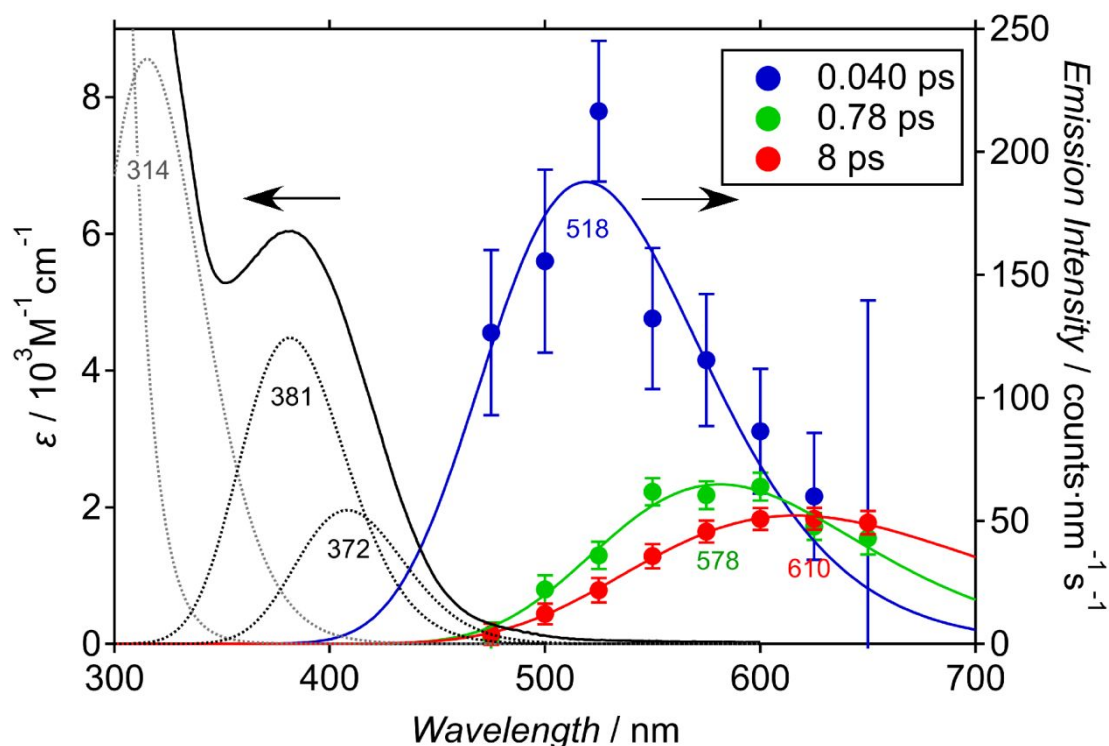
Figure 6. Species-associated fluorescence and absorption spectra of Cu-dimer. Blue: 0.040-ps, Green: 0.78 ps Red 8.0-ps components. Solid lines are fitting curves for the species-associated spectra made from the Gaussian line shape function represented in wavenumber. (λ_{ex} = 405 nm, 4.9×10^{-4} mol/dm^3) Black solid line is the absorption spectrum, where dotted lines are Gaussian line components represented in wavenumber estimated by the Gaussian multi peak fitting to the absorption spectrum. Numbers on the spectra are peak wavelengths (nm) of the absorption or emission bands.

The area intensity of each SAS is proportional to the product of the radiative rate constant (k_r) and the yield of each transition (e.g., $\phi_n \cdot k_{rn}$, see ESI for details). The ratio between the area intensities of the SAS for the $S_{init} \rightarrow S_0$, the $S_1^{IS} \rightarrow S_0$ and $S_1^{FS} \rightarrow S_0$ transitions were estimated as 3.1: 1.0: 1.0. We have already estimated the corrected spectra of the fluorescence and the ^{3}MLCT emission (Figure 3b). The area intensity of the fast emission band is 140 times larger than that of the 97-ns emission component (1.0: 0.0071), supposing the fluorescence intensity recorded in the nanosecond time-resolved emission spectra is dominated by the most long-lived fluorescence component, 8.0-ps components. Therefore, supposing ϕ_1 is also close to unity, k_r of the S_{Init}, S_1^{IS}, S_1^{FS} and T_1^{FS} are estimated to be 3.1 : 1.0 : 1.0 : 0.0071. Using k_r of T_1^{FS} (1.8×10^6 s^{-1}) evaluated from the emission quantum yield (0.041) and its lifetime (1.3×10^4 s^{-1}),[49] k_r for the electronic transition from the S_{Init}, S_1^{IS} and S_1^{FS} to the ground state are estimated as 5.6×10^6 s^{-1}, 1.9×10^6 s^{-1} and 1.8×10^6 s^{-1} respectively. The considerable difference between k_r of the 0.040-ps component (the

$S_{Init} \rightarrow S_0$ transitions, 5.6×10^6 s^{-1}) and that of the 0.78 -ps component (the $S_1 \rightarrow S_0$ transitions, 1.9×10^6 s^{-1}) confirms that these two emitting components are originated from different electronic states (S_{Init} and S_1).   On the other hand, the similarity in k_r for the 0.78 -ps and the 8.0-ps components (1.9×10^6 s^{-1} and 1.8×10^6 s^{-1}) confirms that these are related to the same electronic states (S_1^{IS} and S_1^{FS}).

The absorption band of the $S_{init} \leftarrow S_0$ and $S_1 \leftarrow S_0$ transitions are estimated from multi-peak Gaussian line shapes function to the absorption spectrum, (Figure 6) so that these are mirror images of emission bands of $S_{Init} \rightarrow S_0$ and the $S_1^{IS} \rightarrow S_0$ transitions, respectively. k_rs of the $S_{Init} \leftarrow S_0$ and $S_1 \leftarrow S_0$ transitions at the ground-state structure evaluated from these absorption bands using the Strickler-Berg equation are 3.1×10^7 s^{-1} and 1.1×10^7 s^{-1}, respectively.[19]   It is somewhat larger than those estimated from the time-resolved emission intensities, but still, it roughly agrees with experimental errors in estimating absorption bands and time-resolved emission intensities.   This supports the validities of our analysis for the emission and absorption spectra and the assignments of the fluorescence bands and $\phi_1 = \phi_2 = 1$.

Evaluated photophysical parameters are listed in Table 1.   It is worth noting that the orders of the time constants for the internal conversion, the structural change and intersystem crossing resemble those for the fluorescence decay dynamics of [Cu(dmp)$_2$]$^+$ and its derivatives, respectively (0.040 ps (internal conversion), 0.66 ps (structural change) and 7.4 ps (intersystem crossing) for [Cu(dmp)$_2$]$^+$ in dichloromethane), confirming our assignments.[13]

Table 1.   Photophysical parameters for Cu-dimer in acetonitrile.

States	Absorption			Emission		
	ν_{abs} / 10^3 cm^{-1}	k_r / 10^7 s^{-1}	f	ν_{em} / 10^3 cm^{-1}	k_r / 10^6 s^{-1}	τ / ps
S_{Init}	26.2[a]	3.1[b]	0.041	19.6[a]	5.6	0.040 ± 0.012
S_1^{IS}	24.5[a]	1.1[b]	0.016	18.1[a]	1.9	$0.78 \pm 0.290.78$
S_1^{FS}	-	-	-	17.5[a]	1.8	8.0 ± 0.6
T_1	-	-	-	16.0[a]	0.013[c]	9.7×10^4

a: Results of Gaussian fitting based on absorption or emission intensity represented by wavenumber.

b: Half of the absorption intensity was used to evaluate emission from the dimer complex because the absorption intensity of the dimer is contributed from both two moieties of Cu complexes but the emission is exhibited from one moiety.

c: Estimated from emission quantum yield and emission lifetime for Ar purged solution in ref.49.

3.4. Excited state dynamics of Cu-monomer

Femtosecond fluorescence temporal profiles of Cu-monomer were successfully measured as shown in Figure S3 and Figure S4. Obtained time constants from the global fitting analysis of them were 0.040 ± 0.01 ps, 0.77 ± 0.31 ps and 8.0 ± 2.7 ps as shown in Figure S5 with their SAS. The time constants are very close to those of relevant processes for Cu-dimer though the shift due to the 0.77-ps spectral change looks to be larger than that of the 0.78-ps process of Cu-dimer (Figure S5).

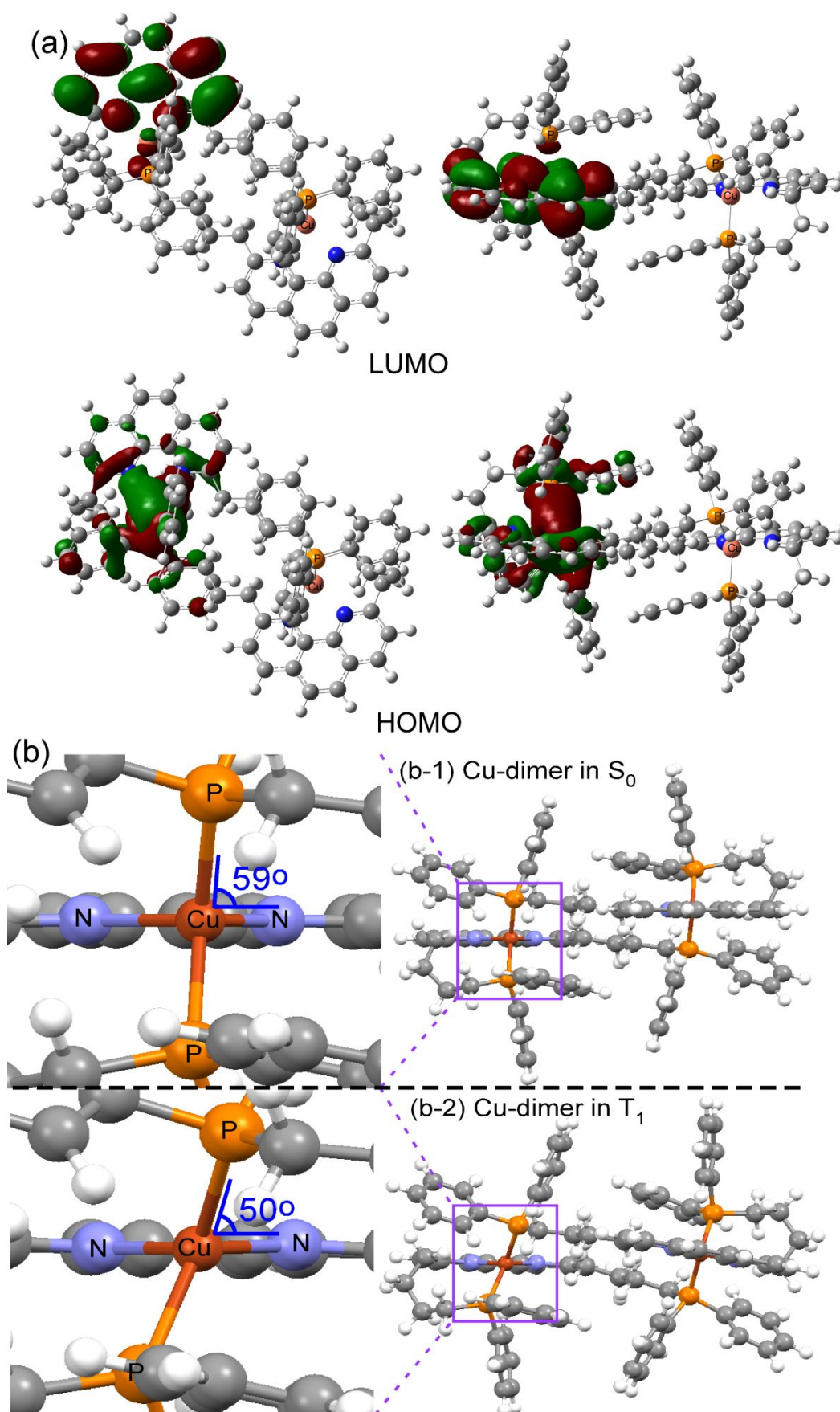### 3.5. Theoretical calculations.

3.5.1. Absorption spectrum

The excited states of the Cu complexes were calculated by the TD-DFT method at the ground state structure. In the calculation, the mononuclear complex (Cu-monomer) was selected as a model system because its spectroscopic features resemble those of Cu-dimer as well as the ultrafast dynamics. The ground state structure of Cu-monomer is close to the crystal structure (See ESI). Four electronic transitions have MLCT characters in the wavelength region around 400 nm. (in Figure S6, details of the electronic transitions with relevant MO are also shown.) Two absorption bands with high intensities are found at 368 nm ($f = 0.034$) and 429 nm ($f = 0.032$) in the calculated absorption data. The upper excited state at 368 nm is characterized by HOMO-2 - LUMO electronic transition and the lower one at 429 nm is by HOMO-LUMO transition. Their k_rs are 1.64×10^7 s^{-1} and 1.17×10^7 s^{-1}, respectively, which are close to those estimated from the absorption bands shown in Figure 6 (3.1×10^7 and 1.1×10^7 s^{-1}, respectively), supporting these states correspond to S_{init} and S_1^{IS}, respectively.

3.5.2. Structural Change Dynamics

The emission peak of S_{Init} is located at 2.43 eV (19600 cm^{-1}), while the absorption peak is located at 3.34 eV (26900 cm^{-1}). The Stokes shift (0.91 eV, 7300 cm^{-1}) at the S_{Init} state indicates that there is an earlier structural change process in the S_{Init} state through spectral change due to the structural change in the S_{Init} was not recognized in the time-resolved fluorescence spectra (Figure 5). This indicates that the structural change in the S_{Init} is too fast to record the relevant emission spectral changes with the fluorescent up-conversion system. We call this earlier structural change in the S_{Init} an 'initial structural change'. After the initial structural change, the S_{Init} relaxed to S_1^{IS} state with the internal conversion. In the S_1 state, another structural change occurs from S_1^{IS} to S_1^{FS} with a time constant of 0.78 ps (slight red shift of the fluorescence from 578 nm to 610 nm, see Fig. 6). We call the 0.78-ps structural change 'following structural change'.

To elucidate the excited-state structural changes of the Cu complexes, the theoretical calculation for Cu-dimer and Cu-monomer was performed for ground state (S_0) and excited state structure (T_1) as shown in Figure 7. The optimized structures of the ground state were obtained to be close to that of the crystal structure.[49] It is found that the frontier orbitals in this structure well represent that the

16

17

HOMO-LUMO transition has an MLCT character (Figure 7).   SCF energy of the ground state (GS) and T_1 (ΔE_{00}, 0-0 excitation energy) are estimated for Cu-dimer and Cu-monomer with their reorganization energy of the structural changes (λ_{st}) as shown in Figure 8. ΔE_{00} and λ_{st} for Cu-dimer are larger (2.44 eV and 0.65 eV) than those of Cu-monomer (2.14 eV and 0.60 eV) as expected from the larger Stokes shift of Cu-dimer than that of Cu-monomer (Figure 2).

(a)

LUMO

HOMO

(b)

(b-1) Cu-dimer in S_0

59°

(b-2) Cu-dimer in T_1

50°

Figure 7. Results of the theoretical calculation for Cu-dimer. (a) Frontier orbitals of Cu-dimer. (b) Structures around the phenanthroline plane and Cu-P-P plane angles of Cu-dimer in GS and T_1
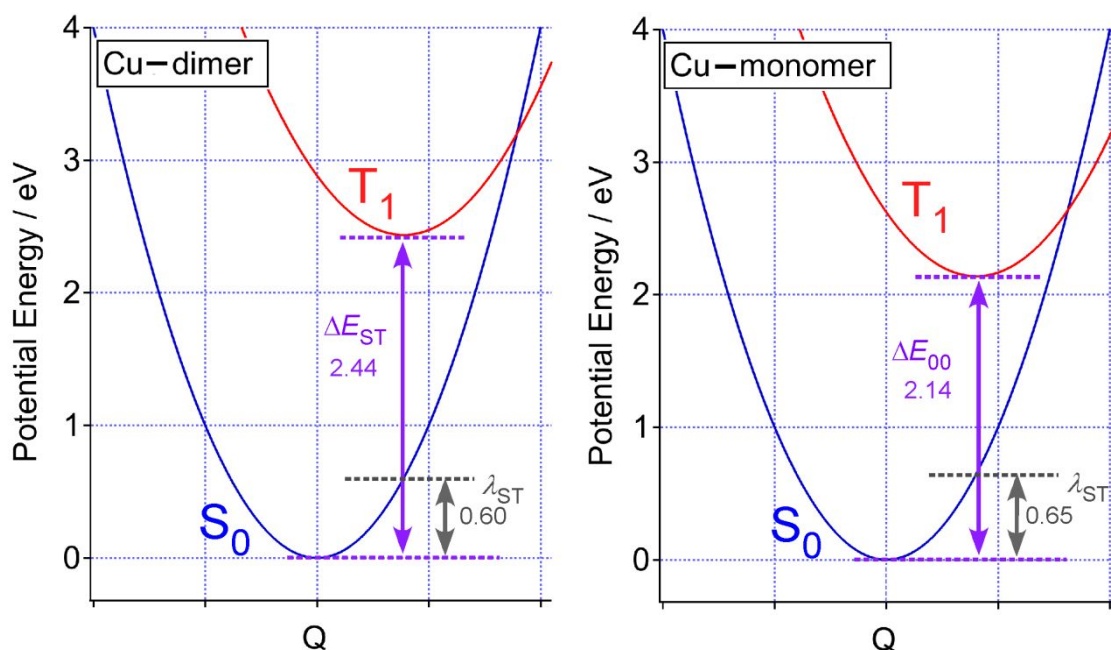
Figure 8. Calculated potential energy diagram of Cu-dimer and Cu-monomer in the ground state (S_0) and the lowst triplet state (T_1). Q is reaction coordinate related with structural change by the photo excitation. ΔE_{00}: 0-0 excitation energy between S_0 and T_1. λ_{st} reorganization energy at S_0 of the structural changes Q.

We found two considerable structural differences between those of S_0 and T_1 in this calculation. One is a flattening distortion due to the Jahn-Teller distortion of the Cu complex induced by the change from Cu(I) to Cu(II) by the MLCT transition. In the T_1 excited state, the dihedral angle between the phenanthroline plane and Cu-P-P plane in Cu-dimer is 50.2°, whereas that of the ground state is 59.0° as shown in Figure 7. (In the case of Cu-monomer, the angle is 71.1° at S_0 and 61.0° at T_1.)

The other one is a structural change in the ligand in the phosphine moiety. The sums of the three bonding angles of C-P-C were estimated to evaluate the degrees of change of phosphine moiety. For the ground state, that in Cu-dimer are 307.7° ~ 308.4°, while two of them are 311.5° in the excited triplet state. Because the excited-state character has some contributions from metal to P charge transition, structural change related to the C-P bond is induced. It is worth noting that the

sum of the three bonding angles of C-P-C is 308.2° ~ 309.2° in the ground state for Cu-monomer, which is almost the same as that of Cu-dimer.   In the case of the excited state, that is 315.4° in the Cu-monomer.

The flattening distortion is assignable to the 'following structural change'.   In the case of Cu(I) bis-diimine complexes, the structural changes of Cu(I) bis-diimine complexes were found to be affected by the viscosity of the solvents.   As mentioned above, the rate of the 'following structural change' is also dependent on the solvents, indicating that it is assignable to the flattening distortion. The time constants of structural change of Cu-dimer and Cu-monomer are ~0.7 ps, which is almost the same as that of flattening structural change of $[Cu(dmp)_2]^+$ in acetonitrile (0.34 ps) in order level, supports the assignment.   The time constants of flattening structural change of Cu(I) diimine complexes are known to be dependent on the bulkiness of the ligand substituents.   For example, those for the structural change are 0.34 ps for $[Cu(dmp)_2]^+$ and 0.2 ps of $[Cu(phen)_2]^+$ in acetonitrile solutions.[15]   Therefore, the somewhat longer time constants for the flattening in Cu-dimer and Cu-monomer (0.78 ps) than those for the simple bis-diimie Cu(I) complexes such as $[Cu(dmp)_2]^+$ (0.34 ps) are due to the bulkier ligands of the Cu-dimer and Cu-monomer than those of the bis-diimie Cu(I) complexes.

The ligand structural changes in C-P-C bond angles are assignable to the 'initial structural change'. Since the P-opening structural change is not sterically hidden, it quickly occurs in the excited state. We estimated the structural relaxation energy in the ligand structure as 0.479 eV for Cu-dimer by calculation of the SCF energy extracted from the calculated structures of GS and T_1.   The experimentally recorded initial Stokes shift (ΔE_{st}) at S_{Init} is 7300 cm^{-1} (0.91 eV, see Table 1), suggesting that reorganization energy in the initial structural change is ~0.46 eV (ΔE_{st} / 2).   This well accords with the calculated reorganization energy in the ligand (0.479 eV) and supports that the initial structural change is dominated by the structural change of the P-opening in the ligand.

The reorganization energy related to the structural change was estimated at 0.602 eV for Cu-dimer (Figure 8).   This is the change of potential energy due to total structural changes (mainly, the sum of the flattening structural change and the ligand structural changes in C-P-C bond angles).   The reorganization energy in the ligand moiety (0.479 eV) indicates that the decrease of potential energy by structural change in the ligand (P-opening) is larger than that in the flattening structural change in $[Cu(I)(N-N)(P)_2]^+$ type complexes.

Finally, the relaxation scheme after the $S_{Init} \leftarrow S_0$ photo-excitation in Cu-dimer with experimentally determined excitation energy of the transition states and time constants of the relaxation processes is represented in Figure 9.   After the photo-excitation of $S_{Init} \leftarrow S_0$ transition, fast structural change in ligand moiety occurs at the S_{Init} state. After it relaxed to the S_1 state with a time constant of 0.040 ps, flattening structural change occurs with a time constant of 0.78 ps.   After that, intersystem crossing occurs in the flattening Cu-dimer with a time constant of 8.0 ps, which

yields triplet Cu-dimer at the flattening structure. Finally, it relaxed to the ground state with a time constant of 97 ns.
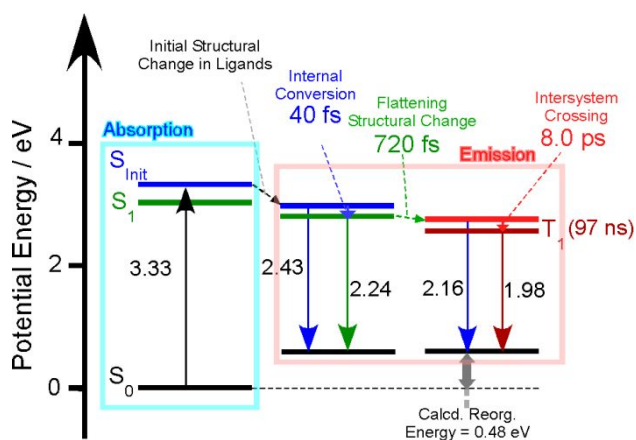
Figure 9. Relaxation process from S_{Init} state in Cu-dimer. Numbers near the arrows representing their electronic transitions are excitation energy of which the unit is eV.

4. Conclusion

Ultrafast relaxation processes of $[Cu(I)(N-N)(P)_2]^+$ were investigated by time-resolved emission spectroscopy. The relaxation process was well reproduced by the tri-exponential function with the three-time constants, e.g. 0.040, 0.78 and 8.0 ps in the case of Cu-dimer. These time constants were assigned to the internal conversion, flattening structural change and intersystem crossing to the triplet state, respectively. These assignments are well consistent with photophysical parameters such as the oscillator strengths estimated from the absorption and emission spectra. While the rates of the flattening structural change for Cu-dimer and Cu-monomer were close to each other, they are slower than that of $[Cu(dmp)_2]^+$.[13] This indicates that the bulkiness of the linked ligands well suppresses the structural change process.

The change of potential energy due to the flattening structural change of Cu-dimer is smaller than that of Cu monomer though the time constants are close to each other. The small change of energy due to the structural changes should be one of the key points for the potential of the photosensitizer of the photo-reduction of CO_2, because the quantum yield of Cu-dimer (smaller structural change) is higher than that of Cu-monomer (larger structural change).[47] The theoretical calculations revealed that the decreases of potential energy by structural changes in the ligands (P-opening) in Cu-dimer and Cu-monomer are larger than that in the flattening structural change in Cu-dimer, which contrasts with homoleptic Cu(I) complexes such as $[Cu(dmp)_2]^+$.[13] Because photo-conversion systems require higher excitation energy of the excited-state photosensitizer, suppressing the initial structural change is important for the development of the system using heteroleptic $[Cu(I)(N-N)(P)_2]^+$.[67]

Conflicts of interest

There are no conflicts to declare.

References

1. K. Kalyanasundaram, *Photochemistry of polypyridine and porphyrin complexes*, Academic Press, London, **1992**.

2. D. M. Roundhill, *Photochemistry and Photophysics of Metal Complexes*, Plenum Publishing Corporation, NewYork and London, 1994.

3. V. Balzani and C. Campagna, *Coordination Compounds I*, Springer, Berlin, 2007.

4. M. Grätzel, *Inorg. Chem.*, 2005, **44**, 6841-6851.

5. V. Balzani, A. Credi and M. Venturi, *ChemSusChem*, 2008, **1**, 26-58.

6. C. L. Linfoot, M. J. Leitl, P. Richardson, A. F. Rausch, O. Chepelin, F. J. White, H. Yersin and N. Robertson, *Inorg. Chem.*, 2014, **53**, 10854-10861.

7. R. Czerwieniec, M. J. Leitl, H. H. Homeier and H. Yersin, *Coord. Chem. Rev.*, 2016, **325**, 2-28.

8. M. J. Leitl, D. M. Zink, A. Schinabeck, T. Baumann, D. Volz and H. Yersin, in *Photoluminescent Materials and Electroluminescent Devices*, Springer 2017, pp. 141-174.

9. A. Tsuboyama, K. Kuge, M. Furugori, S. Okada, M. Hoshino and K. Ueno, *Inorg. Chem.*, 2007, **46**, 1992-2001.

10. D. V. Scaltrito, D. W. Thompson, J. A. O'Callaghan and G. J. Meyer, *Coord. Chem. Rev.*, 2000, **208**, 243-266.

11. N. Armaroli, *Chem. Soc. Rev.*, **2001**, **30**, 113-124.

12. C. S. Ponseca Jr, P. Chabera, J. Uhlig, P. Persson and V. Sundstrom, *Chem. Rev.*, 2017, **117**, 10940-11024.

13. M. Iwamura, S. Takeuchi and T. Tahara, *J. Am. Chem. Soc.*, 2007, **129**, 5248-5256.

14. M. T. Miller, P. K. Gantzel and T. B. Karpishin, *Inorg. Chem.*, 1998, **37**, 2285-2290.

15. M. Iwamura, S. Takeuchi and T. Tahara, *Acc. Chem. Res.*, 2015, **48**, 782-791.

16. L. Duabc and Z. Lan, *Phys. Chem. Chem. Phys*, 2016, **18**, 7641-7650.

17. J. Huang, O. Buyukcakir, M. W. Mara, A. Coskun, N. M. Dimitrijevic, G. Barin, O. Kokhan, A. B. Stickrath, R. Ruppert, D. M. Tiede, J. F. Stoddart, J.-P. Sauvage and L. X. Chen, *Angew. Chem.Int. Ed.*, 2012, **51**, 12711-12715.

18. M. W. Mara, K. A. Fransted and L. X. Chen, *Coord. Chem. Rev.*, 2015, **282-283**, 2-18.

19. Z. A. Siddique, Y. Yamamoto, T. Ohno and K. Nozaki, *Inorg. Chem.*, 2003, **42**, 6366-6378.

20. M. Iwamura, S. Takeuchi and T. Tahara, *Phys. Chem. Chem. Phys*, 2014, **16**, 4143-4154.

21. M. Iwamura, F. Kobayashi and K. Nozaki, *Chem. Lett.*, 2015, **45**, 167-169.

22. T. Gunaratne, M. A. J. Rodgers, D. Felder, J.-F. Nierngarten, G. Accorsi and N. Armaroli, *Chem. Comm.*, 2003, **3010-3011**.

23. M. Iwamura, H. Watanabe, K. Ishii, S. Takeuchi and T. Tahara, *J. Am. Chem. Soc.*, 2011, **133**, 7728-7736.

24. L. Hua, M. Iwamura, S. Takeuchi and T. Tahara, *Phys. Chem. Chem. Phys*, **2015**.

25. S. Garakyaraghi, E. O. Danilov, C. E. McCusker and F. N. Castellano, *J. Phys. Chem. A*, 2015, **119**, 3181-3193.

26. M. C. Rosko, K. A. Wells, C. E. Hauke and F. N. Castellano, *Inorg. Chem.*, 2021, **60**, 8394-8403.

27. I. I. Vorontsov, T. Graber, A. Y. Kovalevsky, ⬚. I. V. Novozhilova, M. Gembicky, Y.-S. Chen and P. Coppens, *J. Am. Chem. Soc.*, 2009, **131**, 6566-6573.

28. J. Huang, M. Mara, A. Stickrath, O. Kokhan, M. Harpham, K. Haldrup, M. Shelby, X. Zhang, R. Ruppert and J.-P. Sauvage, *Dalton Trans.*, 2014, **43**, 17615-17623.

29. T. J. Penfold, S. Karlsson, G. Capano, F. A. Lima, J. Rittmann, M. Reinhard, H. Rittmann-Frank, O. Bram, E. Baranoff, R. Abela, I. Tavernelli, U. Rothlisberger, C. J. Milne and M. Chergui, *J. Phys. Chem. A*, 2013, **117**, 4591–4601.

30. T. Katayama, T. Northey, W. Gawelda, C. J. Milne, G. Vankó, F. A. Lima, R. Bohinc, Z. Németh, S. Nozawa and T. Sato, *Nature commun.*, 2019, **10**, 1-8.

31. G. Smolentsev, A. V. Soldatov and L. X. Chen, *J. Phys. Chem. A*, 2008, **112**, 5363-5367.

32. L. X. Chen, G. B. Shaw, I. Novozhilova, T. Liu, G. Jennings, K. Attenkofer, G. J. Meyer and P. Coppens, *J. Am. Chem. Soc.*, 2003, **125**, 7022-7034.

33. G. Smolentsev, A. V. Soldatov and L. X. Chen, *J. Phys.1 Chem. A*, 2008, **112**, 5363-5367.

34. L. X. Chen, X. Y. Zhang, J. V. Lockard, A. B. Stickrath, K. Attenkofer, G. Jennings and D. J. Liu, *Acta Crystallogr. Sect. A*, 2010, **66**, 240-251.

35. J. V. Lockard, S. Kabehie, J. I. Zink, G. Smolentsev, A. Soldatov and L. X. Chen, *Journal of Physical Chemistry B*, 2010, **114**, 14521-14527.

36. N. A. Gothard, M. W. Mara, J. Huang, J. M. Szarko, B. Rolczynski, J. V. Lockard and L. X. Chen, *J. Phys. Chem. A*, 2012, **116**, 1984-1992.

37. A. Guda, J. Windisch, B. Probst, J. A. Van Bokhoven, R. Alberto, M. Nachtegaal, L.

X. Chen and G. Smolentsev, *Physical Chemistry Chemical Physics*, 2021, **23**, 26729-26736.

38. G. B. Shaw, C. D. Grant, H. Shirota, E. W. CastnerJr., G. J. Meyer and L. X. Chen, *J. Am. Chem. Soc.*, 2007, **129**, 2147-2160.

39. M. W. Mara, B. T. Phelan, Z.-L. Xie, T. W. Kim, D. J. Hsu, X. Liu, A. J. Valentine, P. Kim, X. Li and S.-i. Adachi, *Chem. Sci.*, 2022, **13**, 1715-1724.

40. X. Wang, C. Lv , M. Koyama, M. Kubo and A. Miyamoto, *J. Organomet. Chem.*, 2005, **691**, 551-556.

41. A. Agena, S. Iuchi and M. Higashi, *Chem. Phys. Lett.*, 2017, **679**, 60-65.

42. L. Du and Z. Lan, *Phys. Chem. Chem. Phys.*, 2016, **18**, 7641-7650.

43. L. Hua, M. Iwamura, S. Takeuchi and T. Tahara, *Phys. Chem. Chem. Phys.*, 2015, **17**, 2067-2077.

44. T. Tahara, in *Advances in Multiphoton Processes and Spectroscopy*, World Scientific2004, vol. **16**, pp. 1-71.

45. M. Rentschler, S. Iglesias, M.-A. Schmid, C. Liu, S. Tschierlei, W. Frey, X. Zhang, M. Karnahl and D. Moonshiram, *Chem. Euro. J.*, 2020.

46. D. Moonshiram, P. Garrido‐Barros, C. Gimbert‐Suriñach, A. Picón, C. Liu, X. Zhang, M. Karnahl and A. Llobet, *Chem.Euro. J.*, 2018, **24**, 6464-6472.

47. S. Garakyaraghi, P. Koutnik and F. N. Castellano, *Phys. Chem. Chem. Phys.* 2017, **19**, 16662-16668.

48. C. Gourlaouen and C. Daniel, *Materials*, 2022, **15**, 5222.

49. H. Takeda, K. Ohashi, A. Sekine and O. Ishitani, *J. Am. Chem. Soc.*, 2016, **138**, 4354-4357.

50. Y. Zhang, M. Schulz, M. Wächtler, M. Karnahl and B. Dietzek, *Coord. Chem. Rev.*, 2018, **356**, 127-146.

51. D. Kim, T. G. Gray and T. S. Teets, *Chem. Commun.*, 2022, **58**, 11446-11449.

52. A. Kaeser, M. Mohankumar, J. Mohanraj, F. Monti, M. Holler, J.-J. Cid, O. Moudam, I. Nierengarten, L. Karmazin-Brelot and C. Duhayon, *Inorg. Chem.*, 2013, **52**, 12140-12151.

53. C. Sandoval-Pauker and B. Pinter, *J. Chem. Phys.*, 2022, **157**, 074306.

54. E. Fresta, G. Volpi, M. Milanesio, C. Garino, C. Barolo and R. D. Costa, *Inorg. Chem.*, 2018, **57**, 10469-10479.

55. C. Minozzi, A. Caron, J. C. Grenier‐Petel, J. Santandrea and S. K. Collins, *Angew. Chem. Int. Ed.*, 2018, **57**, 5477-5481.

56. A. Listorti, G. Accorsi, Y. Rio, N. Armaroli, O. Moudam, A. Gégout, B. Delavaux-Nicot, M. Holler and J.-F. Nierengarten, *Inorg. Chem.*, 2008, **47**,

6254-6261.

57.   M. Mohankumar, F. Monti, M. Holler, F. Niess, B. Delavaux‑Nicot, N. Armaroli, J. P. Sauvage and J. F. Nierengarten, *Chem. Euro. J.*, 2014, **20**, 12083-12090.

58.   M. Santander‑Nelli, D. Cortés‑Arriagada, L. Sanhueza and P. Dreyse, *New J. Chem.*, 2022, **46**, 10584-10593.

59.   H. Takeda, H. Kamiyama, K. Okamoto, M. Irimajiri, T. Mizutani, K. Koike, A. Sekine and O. Ishitani, *J. Am. Chem. Soc.*, 2018, **140**, 17241-17254.

60.   H. Takeda, Y. Monma, H. Sugiyama, H. Uekusa and O. Ishitani, *Front. Chem.*, 2019, **7**, 418.

61.   H. Takeda, Y. Monma and O. Ishitani, *ACS Catalysis*, 2021, **11**, 11973-11984.

62.   H. Takeda, A. Kobayashi and K. Tsuge, *Coord. Chem. Rev.*, 2022, **470**, 214700.

63.   M. J. Frisch, G. W. Trucks, H. B. Schlegel, G. E. Scuseria, M. A. Robb, J. R. Cheeseman, G. Scalmani, V. Barone, G. A. Petersson, H. Nakatsuji, X. Li, M. Caricato, A. V. Marenich, J. Bloino, B. G. Janesko, R. Gomperts, B. Mennucci, H. P. Hratchian, J. V. Ortiz, A. F. Izmaylov, J. L. Sonnenberg, Williams, F. Ding, F. Lipparini, F. Egidi, J. Goings, B. Peng, A. Petrone, T. Henderson, D. Ranasinghe, V. G. Zakrzewski, J. Gao, N. Rega, G. Zheng, W. Liang, M. Hada, M. Ehara, K. Toyota, R. Fukuda, J. Hasegawa, M. Ishida, T. Nakajima, Y. Honda, O. Kitao, H. Nakai, T. Vreven, K. Throssell, J. A. Montgomery Jr., J. E. Peralta, F. Ogliaro, M. J. Bearpark, J. J. Heyd, E. N. Brothers, K. N. Kudin, V. N. Staroverov, T. A. Keith, R. Kobayashi, J. Normand, K. Raghavachari, A. P. Rendell, J. C. Burant, S. S. Iyengar, J. Tomasi, M. Cossi, J. M. Millam, M. Klene, C. Adamo, R. Cammi, J. W. Ochterski, R. L. Martin, K. Morokuma, O. Farkas, J. B. Foresman and D. J. Fox, Wallingford, CT2016.

64.   J. P. Perdew, K. Burke and M. Ernzerhof, *Phys. Rev. Lett.*, 1996, **77**, 3865-3868.

65.   C. Adamo and V. Barone, *J. Chem. Phys.*, 1999, **110**, 6158-6169.

66.   J. R. Kirchhoff, R. E. J. Gamache, M. W. Blaskie, A. A. Delpaggio, R. K. Lengel and D. R. McMillin, *Inorg. Chem.*, 1983, **22**, 2380-2384.

67.   M. W. Mara, N. E. Jackson, J. Huang, A. B. Stickrath, X. Y. Zhang, N. A. Gothard, M. A. Ratner and L. X. Chen, *J. Phys.Chem. B*, 2013, **117**, 1921-1931.